Loch Seaforth Marine Modelling Report

Trilleachan Mor

CAR/L/1013016

January 2025

Mowi Scotland

OFFICE
Mowi, Farms Office, Glen Nevis Business Park
PH33 6RX Fort William

POSTAL
Mowi, Farms Office, Glen Nevis Business Park
PH33 6RX Fort William

PHONE

FAX
-

MAIL
environment@mowi.com

WEB
http://mowiscotland.co.uk

CONTENTS

Page

1. INTRODUCTION 6

2. MODEL DESCRIPTION 7

3. CONFIGURATION AND BOUNDARY FORCING FOR LOCH SEAFORTH 8

4. MODEL CALIBRATION AND VALIDATION 11

4.1.1 Near-Surface Current Measurements 11

4.1.2 Model Performance Assessment 11

4.2 Calibration: 17 June – 18 July 2005 (ID435) 11

4.3 Validation: 18 June – 21 September 2024 (ID440) 15

4.4 Validation: 10 September – 08 November 2020 (ID347, ID348) 19

4.4.1 ID347 (Noster) 19

4.4.2 ID348 (Seaforth) 22

5. MODELLED FLOW FIELDS 24

6. CONCLUSIONS 26

7. REFERENCES 26

LIST OF FIGURES

Figure 1. Locations of the Mowi sites in Loch Seaforth (top) and (bottom) the pen locations (●) and current meter deployments (red markers) used in this application. 6

Figure 2. The mesh and domain of the Loch Seaforth model. The pen locations marked (●). 8

Figure 3. *The unstructured mesh around the Trilleachan Mor site, with the cage locations indicated (●).* 9

Figure 4. Model water depths (H, m) in the model domain (right), incorporating multibeam data around the Seaforth and Noster sites. The pen locations at the three Mowi sites are indicated (●). 9

Figure 5. Climatological river flows into Loch Seaforth and the adjacent Loch Claidh used in the modelling. 10

Figure 6. Comparison between observed and modelled sea surface height from ID435 using model parameter values from Table 1. Both the full record (left) and a subset of 15 days (right) are shown. In the latter, the observed data are in blue, model results in red. 12

Figure 7. Comparison between observed and modelled East (left) and North (right) components of velocity at the ADCP location for 15 days in June – July 2005 (ID435) at three depths: 6.9 m (top), 11.9 m (middle) and 32.9 m (2.0 m above the seabed, bottom). Observed data are in blue, model results in red. 13

Figure 8. Histograms of observed and modelled speed (left) and direction (right) at the ADCP location for 15 days in June – July 2005 (ID435) at three depths: 6.9 m (top), 11.9 m (middle) and 32.9 m (2.0 m above the seabed, bottom). Observed data are in blue, model results in red. 14

Figure 9. Scatter plot of observed and modelled velocity at the ADCP location for 15 days in June – July 2005 (ID435) at three depths: 6.9 m (top), 11.9 m (middle) and 32.9 m (2.0 m above the seabed, bottom). Observed data are in blue, model results in red. 14

Figure 10. Comparison between observed and modelled sea surface height from ID440 using model parameter values from Table 1. Both the full record (left) and a subset of 15 days (right) are shown. In the latter, the observed data are in blue, model results in red. 15

Figure 11. Comparison between observed and modelled East (left) and North (right) components of velocity at the ADCP location from 18 June – 21 September 2024 (ID440) at three depths: 3.6 m (top), 5.6 m (middle) and 7.1 m (bottom). Observed data are in blue, model results in red. 16

Figure 12. Histograms of observed and modelled speed (left) and direction (right) at the ADCP location from 18 June – 21 September 2024 (ID440) at three depths: 3.6 m (top), 5.6 m (middle) and 7.1 m (bottom). Observed data are in blue, model results in red. 16

Figure 13. Scatter plot of observed and modelled velocity at the ADCP location from 18 June – 21 September 2024 (ID440) at three depths: 3.6 m (top), 5.6 m (middle) and 7.1 m (bottom). Observed data are in blue, model results in red. 17

Figure 14. Cumulative vector plots of the observed and modelled velocity at the ADCP location from 18 June – 21 September 2024 (ID440) at three depths: 3.6 m (top), 5.6 m (middle) and 7.1 m (bottom). Observed data are in blue, model results in red. 18

Figure 15. Profiles of observed and modelled East (blue) and North (red) components of mean velocity and mean current speed (yellow) from 18th June – 21st September 2024 (ID440). 18

Figure 16. Comparison between observed and modelled sea surface height from ID347 using model parameter values from Table 1. Both the full record (left) and a subset of 15 days (right) are shown. In the latter, the observed data are in blue, model results in red. 19

Figure 17. Comparison between observed and modelled East (left) and North (right) components of velocity at the ADCP location for 15 days in June – July 2020 (ID347) at three depths: 19.3 m (top), 35.3 m (middle) and 65.3 m (4.7 m above the seabed, bottom). Observed data are in blue, model results in red. 20

Figure 18. Histograms of observed and modelled speed (left) and direction (right) at the ADCP location for 15 days in June – July 2020 (ID347) at three depths: 19.3 m (top), 35.3 m (middle) and 65.3 m (4.7 m above the seabed, bottom). Observed data are in blue, model results in red. 20

Figure 19. Scatter plot of observed and modelled velocity at the ADCP location for 15 days in June – July 2020 (ID347) at three depths: 19.3 m (top), 35.3 m (middle) and 65.3 m (4.7 m above the seabed, bottom). Observed data are in blue, model results in red. 21

Figure 20. Comparison between observed and modelled sea surface height from ID348 using model parameter values from Table 1. Both the full record (left) and a subset of 15 days (right) are shown. In the latter, the observed data are in blue, model results in red. 22

Figure 21. Comparison between observed and modelled East (left) and North (right) components of velocity at the ADCP location for 15 days in June – July 2020 (ID348) at

three depths: 26.9 m (top), 46.9 m (middle) and 104.9 m (4.7 m above the seabed, bottom). Observed data are in blue, model results in red. 23

Figure 22. Histograms of observed and modelled speed (left) and direction (right) at the ADCP location for 15 days in June – July 2020 (ID348) at three depths: 26.9 m (top), 46.9 m (middle) and 104.9 m (4.7 m above the seabed, bottom). Observed data are in blue, model results in red. 23

Figure 23. Scatter plot of observed and modelled velocity at the ADCP location for 15 days in June – July 2020 (ID348) at three depths: 26.9 m (top), 46.9 m (middle) and 104.9 m (4.7 m above the seabed, bottom). Observed data are in blue, model results in red. 24

Figure 24. Modelled flood (left) and ebb (right) near-surface current vectors at Trilleachan Mor during spring tides on 21st August 2024 at 18:00Z and 00:00Z respectively. 25

Figure 25. Modelled mean (residual) near-surface current vectors (left) and streamlines (right) at Trilleachan Mor, averaged over the full simulation from 18th June – 21st September 2024. 26

LIST OF TABLES

Table 1. Parameter values chosen for the FVCOM model during the calibration simulations. 12

Table 2. Model performance statistics for sea surface height (SSH) and East and North velocity at the ADCP location from 17 June – 18 July 2005 (ID435) at three depths (6.9 m, 11.9 m and 32.9 m).* 13

Table 3. Model performance statistics for sea surface height (SSH) and East and North velocity at the ADCP location from 18 June – 21 September 2024 (ID440) at three depths (3.6 m, 5.6 m and 7.1 m)......15

Table 4. Model performance statistics for sea surface height (SSH) and East and North velocity at the ADCP location from 10 September – 08 November 2020 (ID347) at three depths (19.3 m, 35.3 m and 65.3 m).* 21

Table 5. Model performance statistics for sea surface height (SSH) and East and North velocity at the ADCP location from 10 September – 08 November 2020 (ID348) at three depths (26.9 m, 46.9 m and 104.9 m).* 22

QUALITY ASSURANCE

Mowi Scotland Ltd is ISO9001 and ISO14001 accredited and all project management follows policies designed to ensure that the collection, collation and reporting of information produced in the course of our operations is done to a consistently high standard meeting the requirements of the end user.

1. Introduction

This report has been prepared by Mowi Scotland Ltd. to meet the requirements of the Scottish Environment Protection Agency (SEPA) for an application to use topical sealice veterinary medicines at the **Trilleachan Mor** marine salmon farm in **Loch Seaforth** (Figure 1). The application uses coupled hydrodynamic and particle tracking modelling to describe the dispersion of bath treatments in order to determine EQS-compliant quantities for the current site biomass and equipment. This report describes the configuration, calibration and validation of the hydrodynamic model used in the application. The dispersion modelling for the site will be described in a separate report.

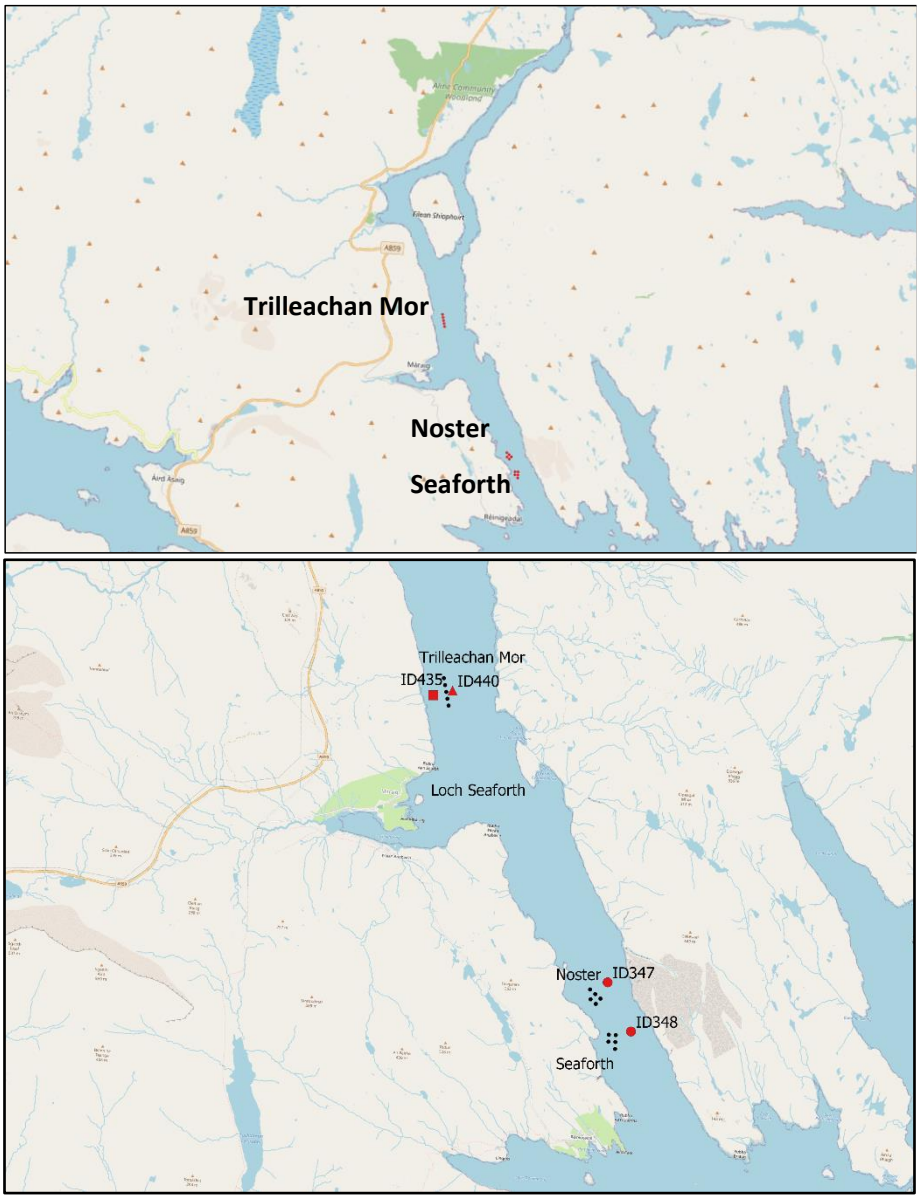

Figure 1. Locations of the Mowi sites in Loch Seaforth (top) and (bottom) the pen locations (●) and current meter deployments (red markers) used in this application.

2. Model Description

The hydrodynamic model used was FVCOM (Finite Volume Community Ocean Model), a prognostic, unstructured-grid, finite-volume, free-surface, 3-D primitive equation coastal ocean circulation model developed by the University of Massachusetts School of Marine Science and the Woods Hole Oceanographic Institute (Chen et al., 2003). The model consists of equations describing the evolution and conservation of momentum, temperature, salinity and turbulence parameters, the latter using a turbulence closure submodel. The horizontal grid is comprised of unstructured triangular cells and the irregular bottom is presented using generalized terrain-following coordinates. The General Ocean Turbulent Model (GOTM) developed by Burchard's research group in Germany (Burchard, 2002) has been added to FVCOM to provide optional vertical turbulent closure schemes. Horizontal viscosity and diffusivity was calculated using the Smagorinsky algorithm, with a coefficient value c_s. FVCOM is solved numerically by a second-order accurate discrete flux calculation in the integral form of the governing equations over an unstructured triangular grid. This approach combines the best features of finite-element methods (grid flexibility) and finite-difference methods (numerical efficiency and code simplicity) and provides a much better numerical representation of both local and global momentum, mass, salt, heat, and tracer conservation. The ability of FVCOM to accurately solve scalar conservation equations in addition to the topological flexibility provided by unstructured meshes and the simplicity of the coding structure has make FVCOM ideally suited for many coastal and interdisciplinary scientific applications, such as typically found in Scotland. The mesh flexibility allows greater spatial resolution in near-shore areas without excessive computational demand.

The model is forced by a tidal condition along the open boundary, and by frictional stresses at the surface and seabed. At the seabed, the frictional stress, $\boldsymbol{\tau}_b$, is calculated using a quadratic equation where:

$$\tau_b = \rho C_D \boldsymbol{U}|\boldsymbol{U}| \quad (1)$$

where ρ = 1025 kg m^{-3} is the water density, **U** is the velocity in the layer closest to the seabed. The drag coefficient, C_D, is calculated from the bed roughness lengthscale, z_0, using:

$$C_D = \left(\frac{\kappa}{\ln\left(\frac{z_b + z_0}{z_0}\right)}\right)^2 \quad (2)$$

where κ=0.4 is von Karman's constant, and z_b is the height above the bed of the lowest velocity point. The value of z_0 was varied during calibration to provide the best fit to observations of sea level and velocity.

Wind forcing is applied as a surface stress calculated from hourly wind speed and direction. Wind stress is calculated from the wind velocity by a standard quadratic relation:

$$\tau_x = \rho_a C_W u W \quad (3a)$$
$$\tau_y = \rho_a C_W v W \quad (3b)$$

where (u,v) are the East and North components of wind velocity respectively, W is the wind speed ($W = [u^2+v^2]^{½}$), ρ_a is the density of air, and the surface drag coefficient C_W is calculated following Large and Pond (1981).

3. Configuration and Boundary Forcing for Loch Seaforth

The Trilleachan Mor site is located in Loch Seaforth in the Western Isles (Figure 1). The unstructured mesh used in the model covered Loch Seaforth and adjacent coastal waters (Figure 2). Model resolution was enhanced within Loch Seaforth, particularly around the Mowi sites at Trilleachan Mor (Figure 3), Noster and Seaforth.

The spatial resolution of the model varied from about 10 m in some inshore waters to about 500 m along the open boundary. The mesh was refined down to about 15 – 20 m in the area of the pens. In total, the model consisted of 30,147 nodes and 57,668 triangular elements.

Model bathymetry was taken from the UK Admiralty Seabed Mapping Service (https://www.admiralty.co.uk/access-data), supplemented by a multibeam survey undertaken around the Seaforth and Noster sites in December 2020 (Figure 4).

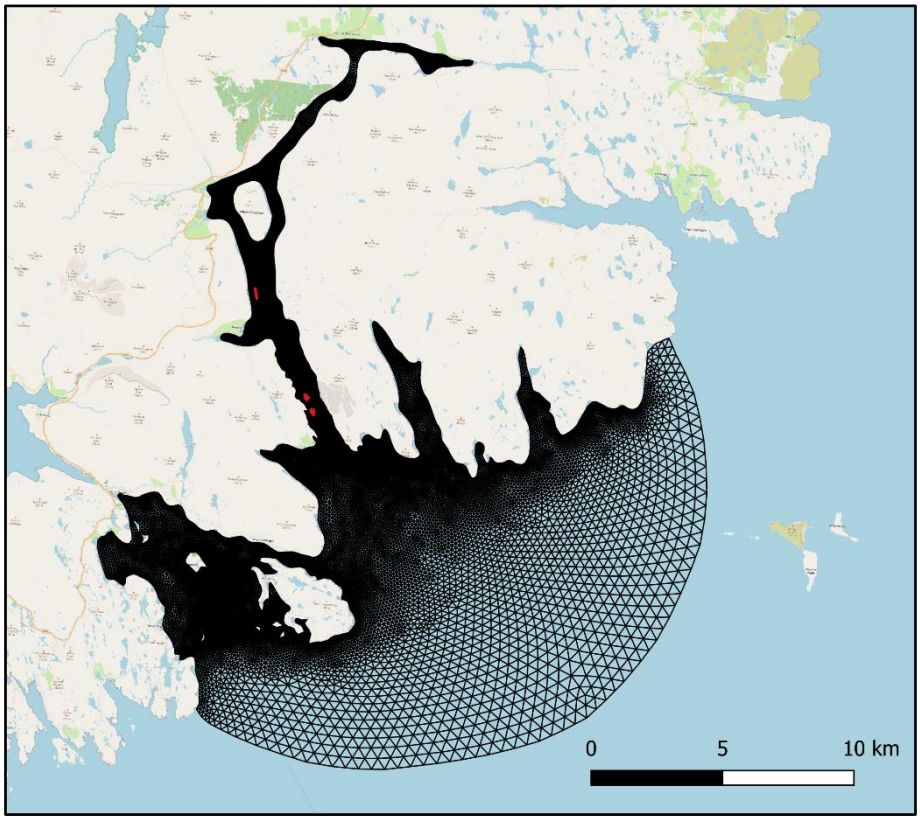

Figure 2. The mesh and domain of the Loch Seaforth model. The pen locations marked (●).

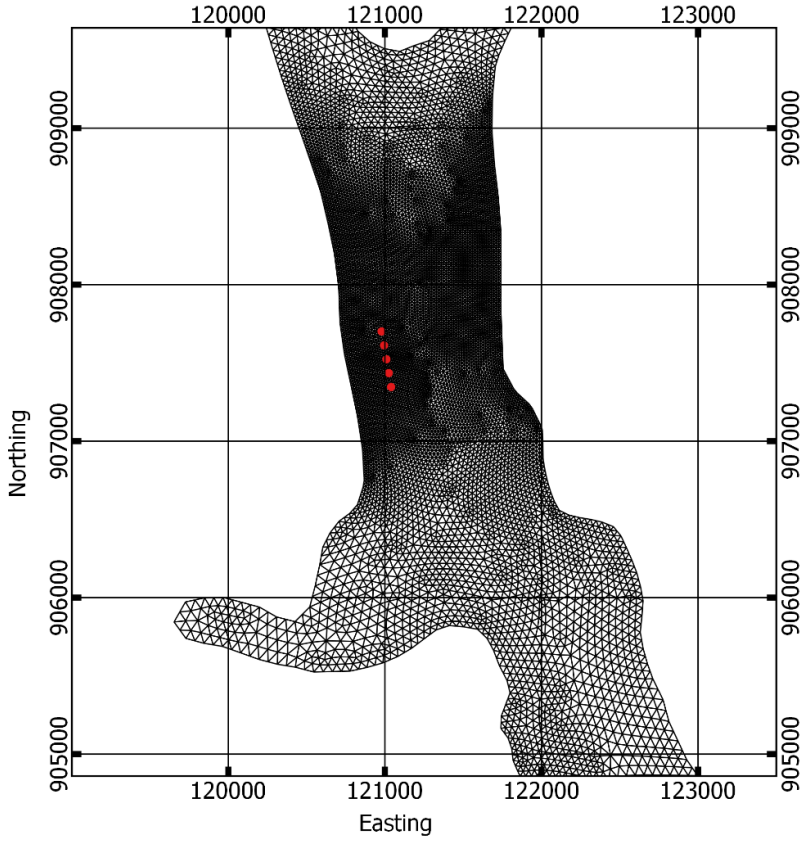

Figure 3. *The unstructured mesh around the Trilleachan Mor site, with the cage locations indicated (●).*

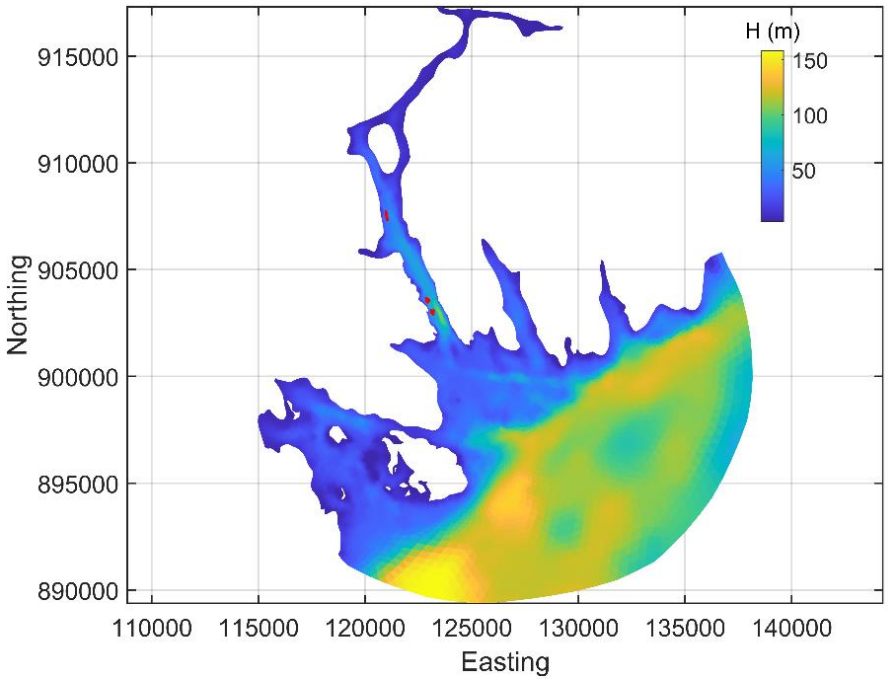

Figure 4. Model water depths (H, m) in the model domain (right), incorporating multibeam data around the Seaforth and Noster sites. The pen locations at the three Mowi sites are indicated (●).

The model was forced along its open boundary by time series of sea surface height (SSH) at each boundary node for the relevant simulation periods; FVCOM appears to perform better when boundary forcing is applied as a time series rather than when tidal constituents are used. The SSH time series were generated using the RiCOM hydrodynamic model (Walters and Casulli, 1998; Gillibrand et al., 2016) on the Scottish Shelf Model ECLH grid (Marine Scotland, 2016), which was, in turn, forced by eight tidal constituents (O_1, K_1, Q_1, P_1, M_2, S_2, N_2, K_2) taken from the full Scottish Shelf model (SSM).

Spatially- and temporally-varying wind speed and direction data were taken from the ERA5 global reanalysis dataset (ECMWF, 2021) for the required simulation periods and interpolated spatially onto the model mesh element centre locations.

Stratification is expected to be moderate in this location and the model was run in 3D baroclinic mode. Fourteen layers in the vertical (fifteen sigma levels) were used in the simulations, with layers concentrated near the surface and seabed. The sigma levels used were:

σ = [0 -0.01 -0.04 -0.09 -0.16 -0.26 -0.37 -0.50 -0.63 -0.74 -0.84 -0.91 -0.96 -0.99 -1.0]

Climatological river flow data were used, taken from the Marine Scotland Scottish Shelf Model climatology (Marine Scotland, 2016). Two freshwater discharges into the model domain were specified (Figure 2), discharging directly into Loch Seaforth and Loch Claidh. The annual climatological river flows into the model domain are shown in Figure 5. The annual-mean flows are comparable to the annual runoff discharges given by Edwards and Sharples (1986).

In the vertical, a general length-scale (gls) turbulence closure scheme was used (Umlauf and Burchard, 2003; Warner et al., 2005). The closure scheme requires bed and surface roughness lengthscales to be specified; these parameters were refined during the calibration process.

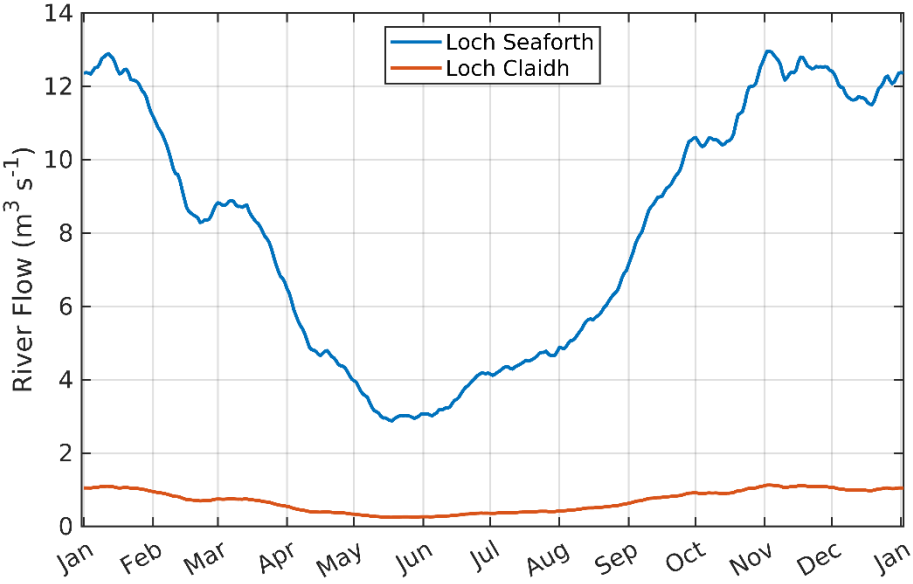

Figure 5. Climatological river flows into Loch Seaforth and the adjacent Loch Claidh used in the modelling.

4. Model Calibration and Validation

The hydrodynamic model was calibrated against current data and seabed pressure data, measured in Loch Seaforth area using Acoustic Doppler Current Profilers (ADCP,Figure 1). Data were available from:

(i) Calibration: 17 June – 18 July 2005 (ID435)
(ii) Validation: 18 June – 21 September 2024 (ID440)
(iii) Validation: 10 September – 08 November 2020 (ID347, ID348)

In total, the data extend over 244 days. The model will be run in 3D, and calibration will be performed primarily by adjusting the bed roughness length scale, z_0, and the horizontal viscosity coefficient, c_s, to obtain the best fit against the sea surface height and current data. Once the best comparison with the calibration data has been achieved, the parameter set will be tested without further adjustment against the validation datasets.

4.1.1 Near-Surface Current Measurements

Deployment ID440 listed above used a Nortek Signature 1000 ADCP instrument (Nortek, 2023). The objective of these measurements was to more accurately measure the currents in the near-surface region of the water column, where bath medicines are applied and disperse following traditional tarp treatments. The Nortek Signature 1000 is a high frequency (1 MHz) ADCP, allowing smaller cell sizes (0.2 – 2.0 m) and higher frequency sampling. The instrument was deployed at mid-depth, *ca.* 8 m below mean sea level (MSL), meaning that less of the sub-surface water column was lost to side-lobe reflections; measurements were made to within about 1 m of the water surface.

For this application, the data were processed in a standard fashion. The near-surface cell was selected as the shallowest cell which contained valid data throughout the deployment. The diagnostic data suggested that velocities from the first 8 bins were valid at all times (Mowi, 2024), therefore data from cell 8 was selected as the near-surface cell. The other cells selected for HG analysis were cells 1 and 4, at depths ~7.0 m and ~5.5 m respectively.

4.1.2 Model Performance Assessment

Model performance is assessed using three metrics: the mean absolute error (MAE), the root-mean-square error (RMSE) and the model skill (d_2). The first two are standard measures of model accuracy; the third, d_2, is taken from Willmott et al. (1985) and lies in the range $0 \leq d_2 \leq 1$, with $d_2 = 0$ implying zero model skill and $d_2 = 1$ indicating perfect skill.

4.2 Calibration: 17 June – 18 July 2005 (ID435)

The calibration used observed depth and current velocity from an historic ADCP deployment to compare with modelled sea surface height (SSH) and velocity (ADCP deployments ID435). The model was calibrated by varying the value of the bed roughness lengthscale, z_0, and the horizontal viscosity coefficient, c_s. Simulations were performed with a range of values of both parameters. After a number of simulations, a final parameter set was selected (Table 1).

Table 1. Parameter values chosen for the FVCOM model during the calibration simulations.

Parameter Description	Value
Bed roughness lengthscale, z_0 (m)	0.01
Smagorinsky coefficient, c_s (m^2 s^{-1})	0.2
Number of vertical layers	14
Barotropic time step (s)	0.5
Baroclinic time step (s)	2.5

The results of the calibration exercise for ID435 are presented in Figure 16 – Figure 18 and Table 4. At the ADCP location, the sea surface height was accurately modelled, with model skill of 1.0. The mean absolute error (MAE) and root-mean-square error (RMSE) values of 0.12 m and 0.14 respectively are about 2.7% and 3.1% of the spring tide range (~4.5 m) respectively.

For the calibration period, the model skill scores were 0.36 and 0.67 for the East and North components of near-surface (6.9 m) velocity respectively, with RMSE values of 0.04 m s^{-1} and 0.07 m s^{-1} for the two components of velocity respectively (Table 4). At the deeper depth of 11.9 m, the skill scores were similar, at 0.32 and 0.78 respectively. The MAE and RMSE values were less than those at the shallower depth, at 0.03 m s^{-1} and 0.06 m s^{-1} respectively. Model performance at the deepest depth were similar (Table 4).

The histograms and scatter plots (Figure 19 and Figure 18) demonstrate that the modelled current had broadly the same magnitude and direction characteristics as the observed data.

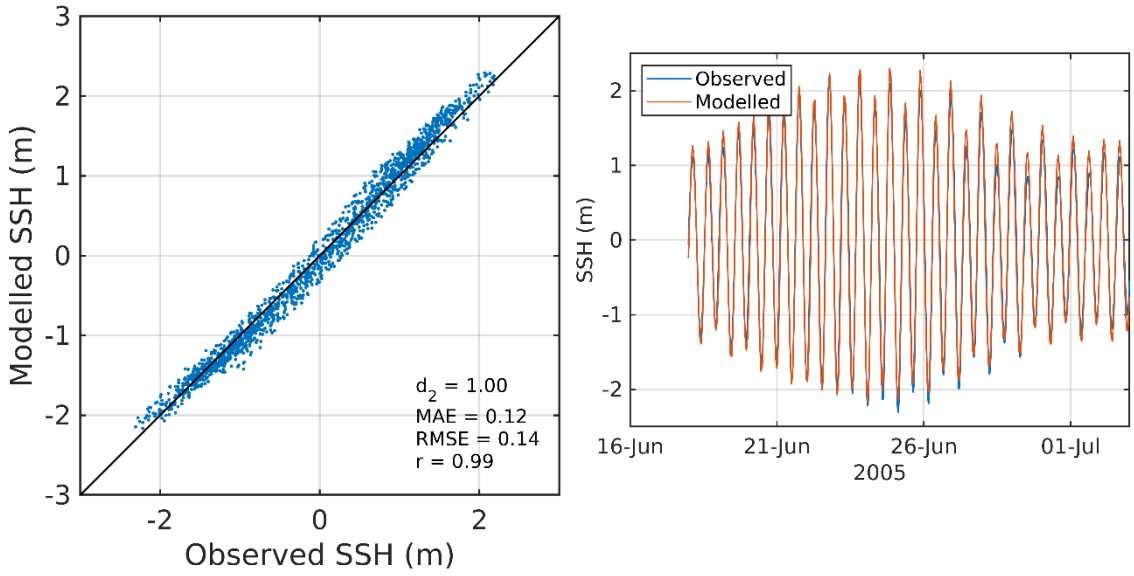

Figure 6. Comparison between observed and modelled sea surface height from ID435 using model parameter values from Table 1. Both the full record (left) and a subset of 15 days (right) are shown. In the latter, the observed data are in blue, model results in red.

Table 2. Model performance statistics for sea surface height (SSH) and East and North velocity at the ADCP location from 17 June – 18 July 2005 (ID435) at three depths (6.9 m, 11.9 m and 32.9 m).*

		Skill, d_2	MAE	RMSE
Sea Surface Height (SSH, m)		1.00	0.12	0.14
6.9 m	East Velocity (m s^{-1})	0.36	0.03	0.04
	North Velocity (m s^{-1})	0.67	0.06	0.07
11.9 m	East Velocity (m s^{-1})	0.32	0.03	0.03
	North Velocity (m s^{-1})	0.78	0.04	0.06
32.9 m*	East Velocity (m s^{-1})	0.37	0.03	0.03
	North Velocity (m s^{-1})	0.59	0.04	0.05

** estimated from mean water depth of 34.9 m*

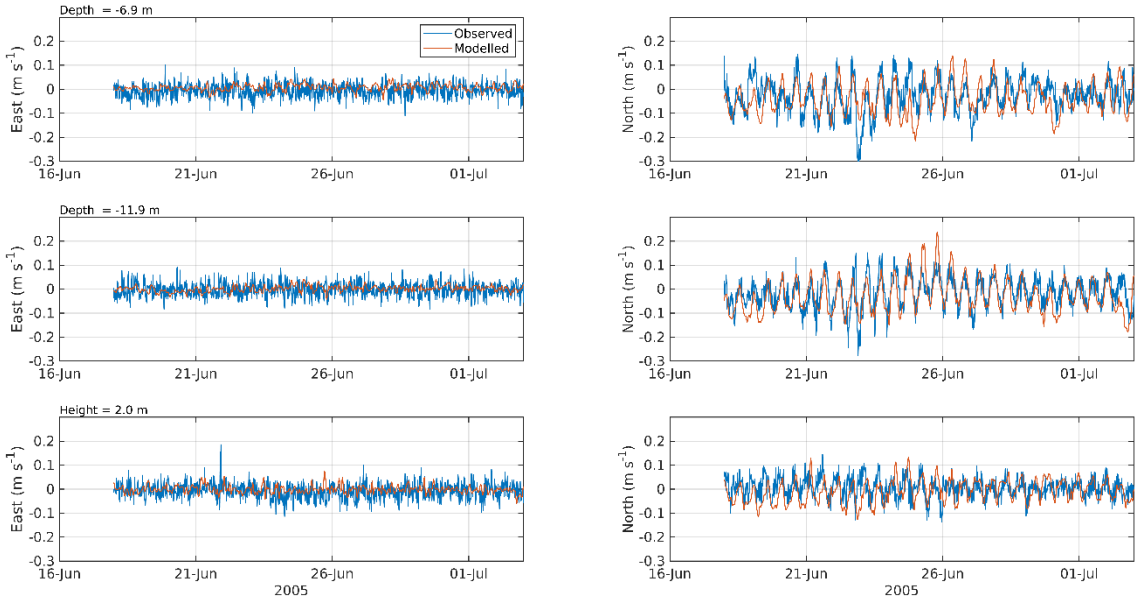

Figure 7. Comparison between observed and modelled East (left) and North (right) components of velocity at the ADCP location for 15 days in June – July 2005 (ID435) at three depths: 6.9 m (top), 11.9 m (middle) and 32.9 m (2.0 m above the seabed, bottom). Observed data are in blue, model results in red.

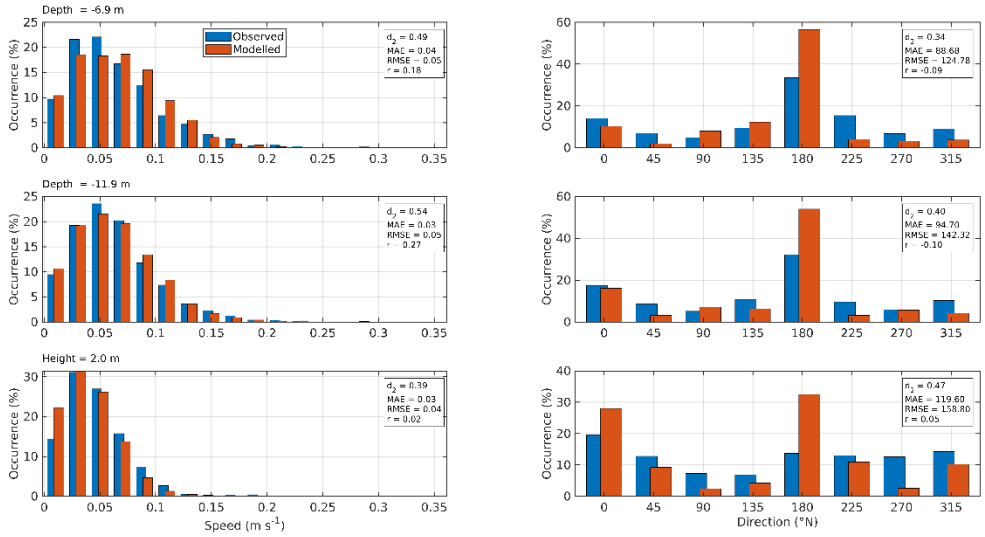

Figure 8. Histograms of observed and modelled speed (left) and direction (right) at the ADCP location for 15 days in June – July 2005 (ID435) at three depths: 6.9 m (top), 11.9 m (middle) and 32.9 m (2.0 m above the seabed, bottom). Observed data are in blue, model results in red.

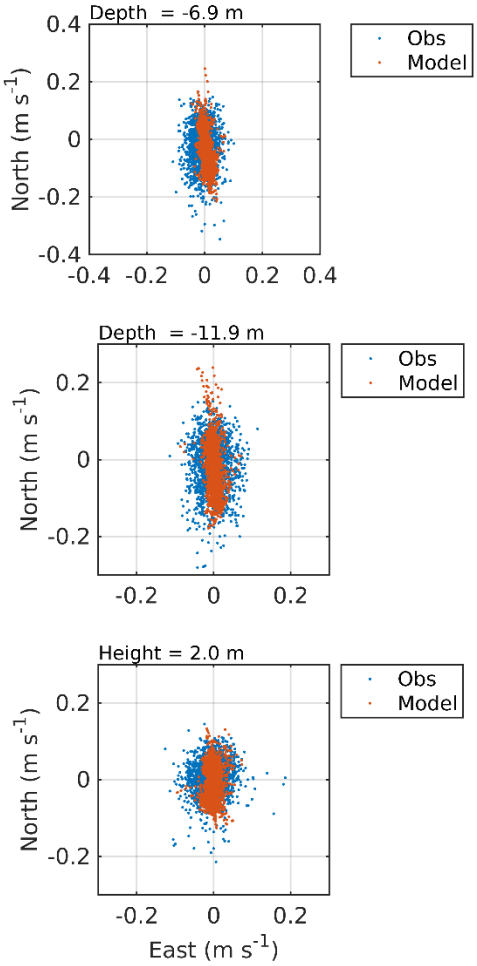

Figure 9. Scatter plot of observed and modelled velocity at the ADCP location for 15 days in June – July 2005 (ID435) at three depths: 6.9 m (top), 11.9 m (middle) and 32.9 m (2.0 m above the seabed, bottom). Observed data are in blue, model results in red.

4.3 Validation: 18 June – 21 September 2024 (ID440)

For the first validation period, the sea surface height was accurately modelled, with model skill of 1.0 (Figure 10, Table 3). The mean absolute error (MAE) and root-mean-square error (RMSE) values of 0.11 m and 0.14 respectively are about 2.4% and 3.1% of the spring tide range (~4.5 m) respectively. Modelled and observed current velocity at three depths are compared in Figure 11 – Figure 13. Model skill scores were 0.42 and 0.70 for the East and North components of near-surface (3.6 m) velocity respectively, with RMSE values of 0.04 m s^{-1} and 0.08 m s^{-1} for the two components of velocity respectively (Table 4). At the deeper depths of 5.6 m and 7.1 m, the skill scores, and MAE and RMSE values were all similar to those at the shallower depth.

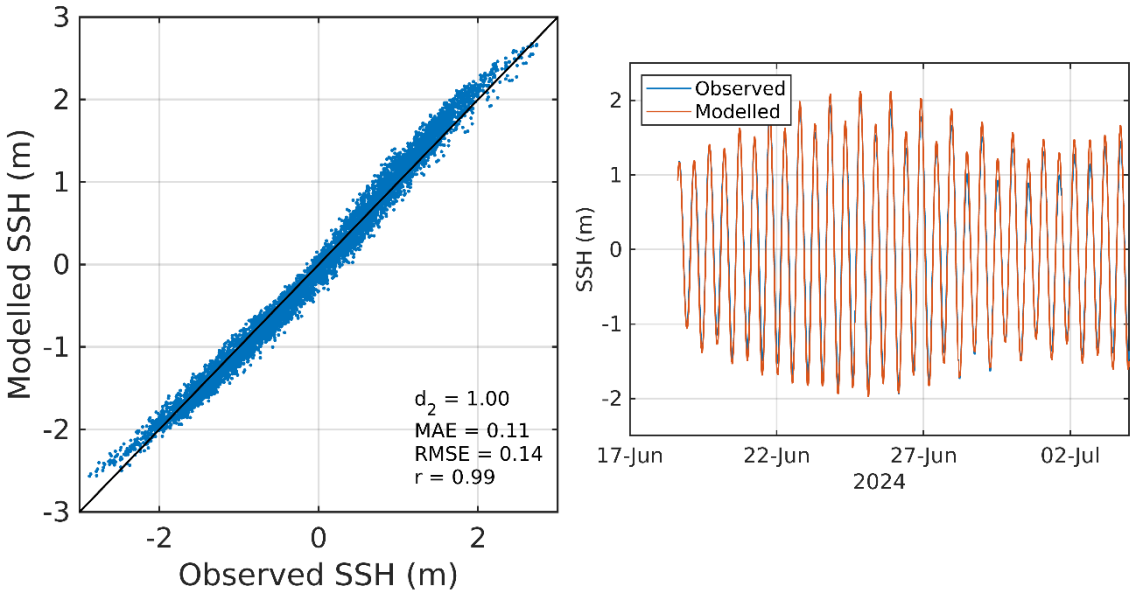

Figure 10. Comparison between observed and modelled sea surface height from ID440 using model parameter values from Table 1. Both the full record (left) and a subset of 15 days (right) are shown. In the latter, the observed data are in blue, model results in red.

Table 3. Model performance statistics for sea surface height (SSH) and East and North velocity at the ADCP location from 18 June – 21 September 2024 (ID440) at three depths (3.6 m, 5.6 m and 7.1 m).

		Skill, d_2	MAE	RMSE
Sea Surface Height (SSH, m)		1.00	0.11	0.14
3.6 m	East Velocity (m s^{-1})	0.42	0.03	0.04
	North Velocity (m s^{-1})	0.70	0.06	0.08
5.6 m	East Velocity (m s^{-1})	0.45	0.03	0.04
	North Velocity (m s^{-1})	0.69	0.05	0.07
7.1 m	East Velocity (m s^{-1})	0.47	0.02	0.03
	North Velocity (m s^{-1})	0.74	0.05	0.06

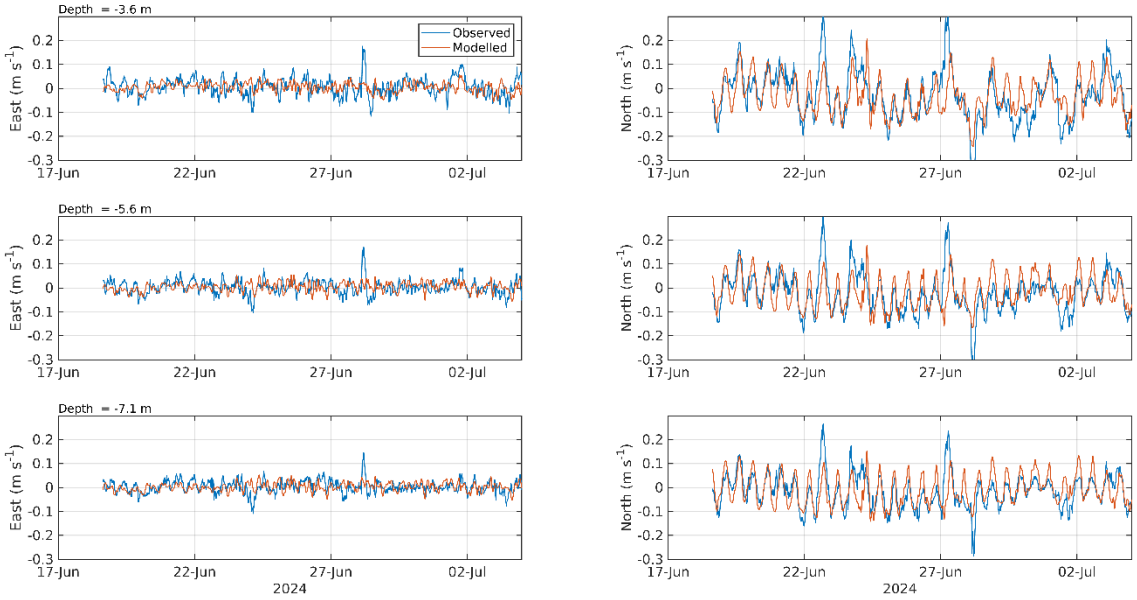

Figure 11. Comparison between observed and modelled East (left) and North (right) components of velocity at the ADCP location from 18 June – 21 September 2024 (ID440) at three depths: 3.6 m (top), 5.6 m (middle) and 7.1 m (bottom). Observed data are in blue, model results in red.

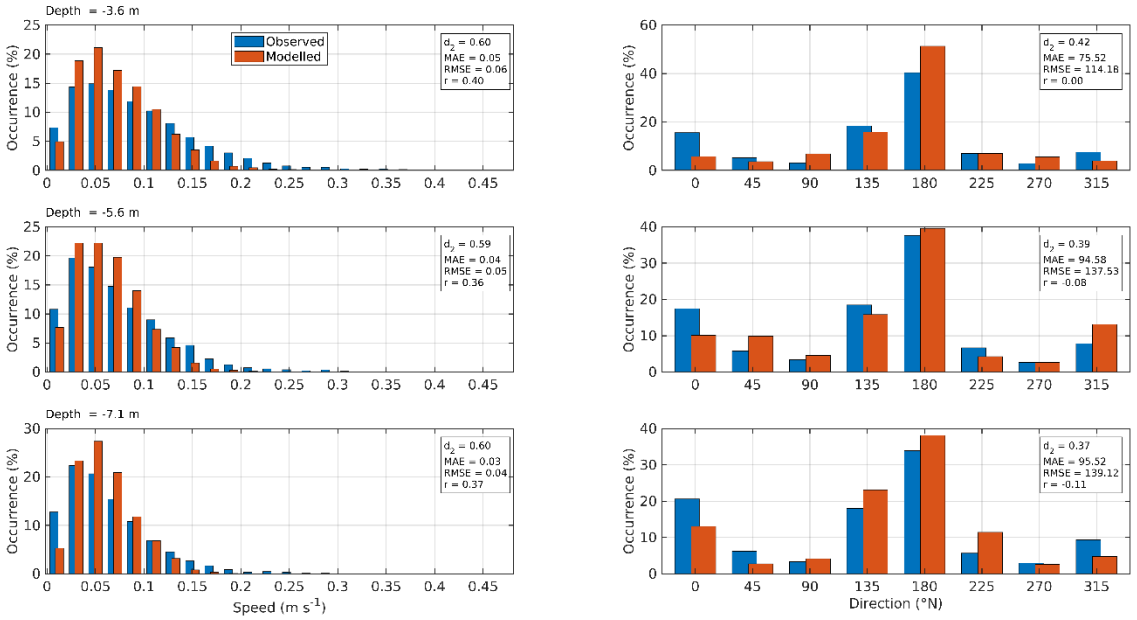

Figure 12. Histograms of observed and modelled speed (left) and direction (right) at the ADCP location from 18 June – 21 September 2024 (ID440) at three depths: 3.6 m (top), 5.6 m (middle) and 7.1 m (bottom). Observed data are in blue, model results in red.

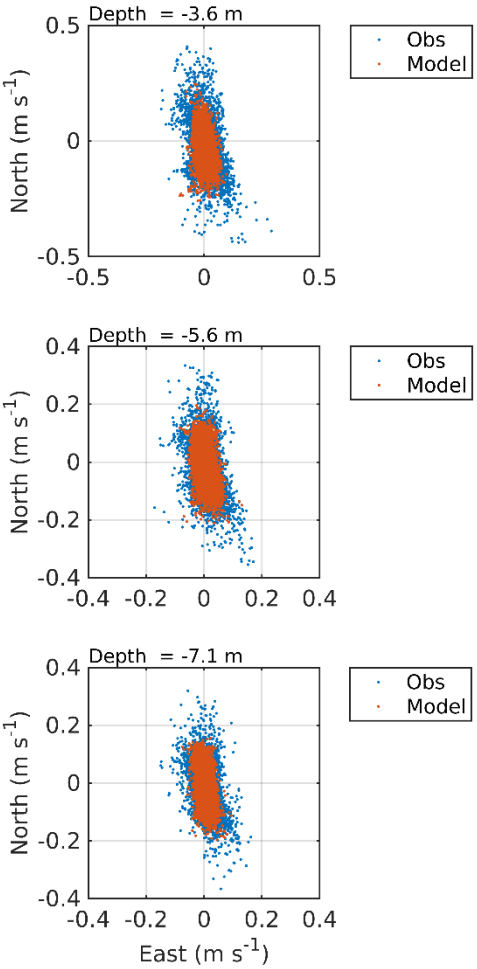

Figure 13. Scatter plot of observed and modelled velocity at the ADCP location from 18 June – 21 September 2024 (ID440) at three depths: 3.6 m (top), 5.6 m (middle) and 7.1 m (bottom). Observed data are in blue, model results in red.

The near-surface currents recorded by the Signature instrument are challenging to model accurately as the stratified surface layer is likely to be highly mobile in response to short-term fluctuations in wind speed and direction and river discharges; perhaps not surprisingly, the observations contained more variability than was found in the modelled currents. However, the histograms and scatter plots (Figure 12 and Figure 13) demonstrate that the modelled current had broadly the same magnitude and direction characteristics as the observed data. Further, transport of patches of medicine following release is driven by the residual (non-tidal) flows, and the comparison of modelled and observed cumulative vector plots in Figure 14 demonstrates that the model is reproducing the near-surface (3.6 m depth) residual flow very well, giving confidence in the suitability of the model flow fields for simulating bath medicine transport and dispersion. The measured near-surface residual flow speed was 3.8 cm s^{-1} (Mowi, 2024), with the modelled residual speed comparing well at 4.2 cm s^{-1} in the same prevailing SSE direction (Figure 14 top).

Finally, the vertical profiles of mean velocity and speed (Figure 15) averaged over the full deployment and simulation period from 18th June – 21st September 2024, demonstrate that the observations from the Signature and the modelled velocity profiles are mutually consistent. This provides confidence in both observations and data.

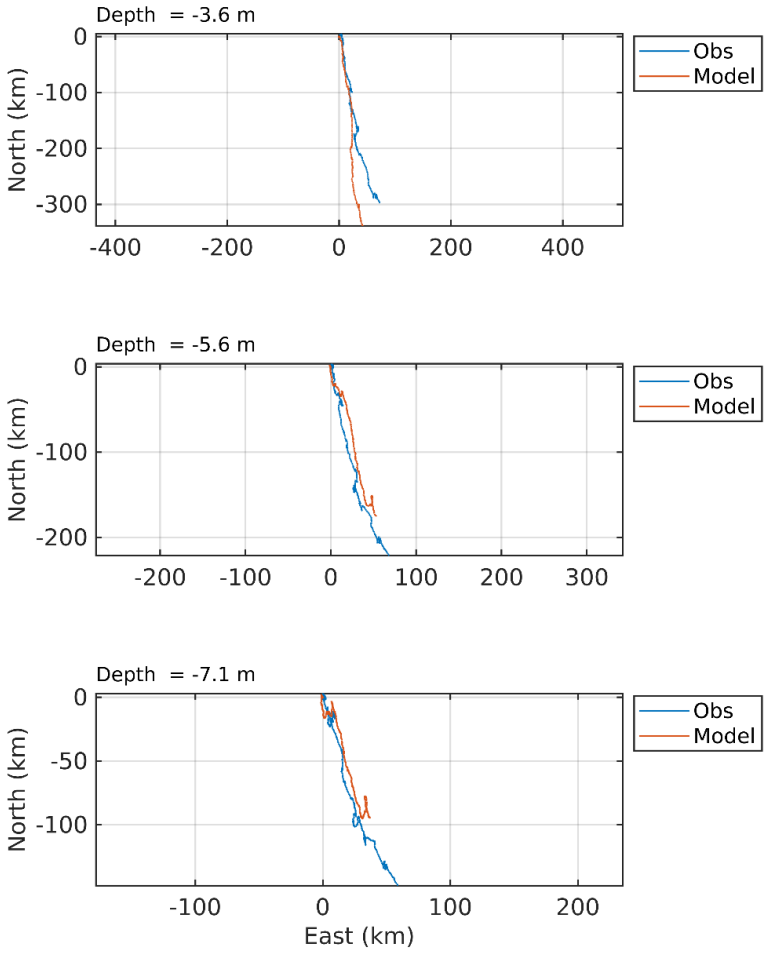

Figure 14. Cumulative vector plots of the observed and modelled velocity at the ADCP location from 18 June – 21 September 2024 (ID440) at three depths: 3.6 m (top), 5.6 m (middle) and 7.1 m (bottom). Observed data are in blue, model results in red.

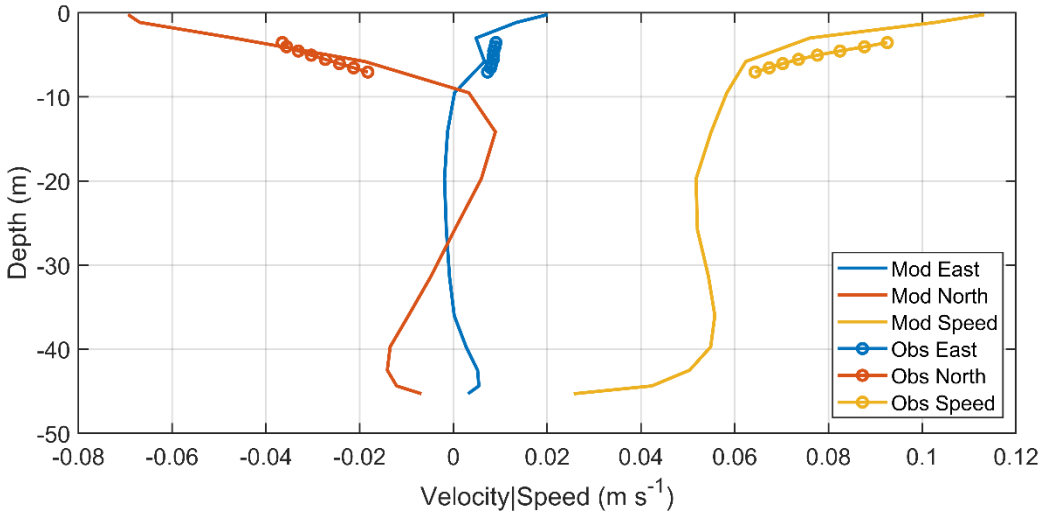

Figure 15. Profiles of observed and modelled East (blue) and North (red) components of mean velocity and mean current speed (yellow) from 18th June – 21st September 2024 (ID440).

4.4 Validation: 10 September – 08 November 2020 (ID347, ID348)

Given that patches of bath medicine released from Trilleachan Mor are likely to be transported south-eastwards, as evidenced by Figure 14 and consistent with the well-understood circulation dynamics of Scottish sea lochs, the final validation simulation used data from two ADCP deployments at the Seaforth and Noster sites in Loch Seaforth (Figure 1); these data were collected in 2020.

4.4.1 ID347 (Noster)

The results of the validation exercise for ID347 are presented in Figure 16 – Figure 19 and Table 4. At the ADCP location, the sea surface height was accurately modelled, with model skill of 1.00. The mean absolute error (MAE) and root-mean-square error (RMSE) values of 0.11 m and 0.14 respectively are about 2.4% and 3.1% of the spring tide range respectively.

Model skill scores for the East and North components of near-surface (19.3 m) velocity were 0.62 and 0.86 respectively, with RMSE values of 0.03 m s^{-1} and 0.05 m s^{-1} for the two components of velocity respectively (Table 4). At the deeper depth of 35.3 m, the skill scores were similar, at 0.58 and 0.85 respectively. The RMSE values were the same as those at the shallower depth, at 0.03 m s^{-1} and 0.05 m s^{-1} respectively. At the deepest depth, 65.3 m, skill scores and RMSE values were similar to those at the shallower depths for both components of velocity.

The histograms and scatter plots (Figure 18 and Figure 19) demonstrate that the modelled current had broadly the same magnitude and direction characteristics as the observed data.

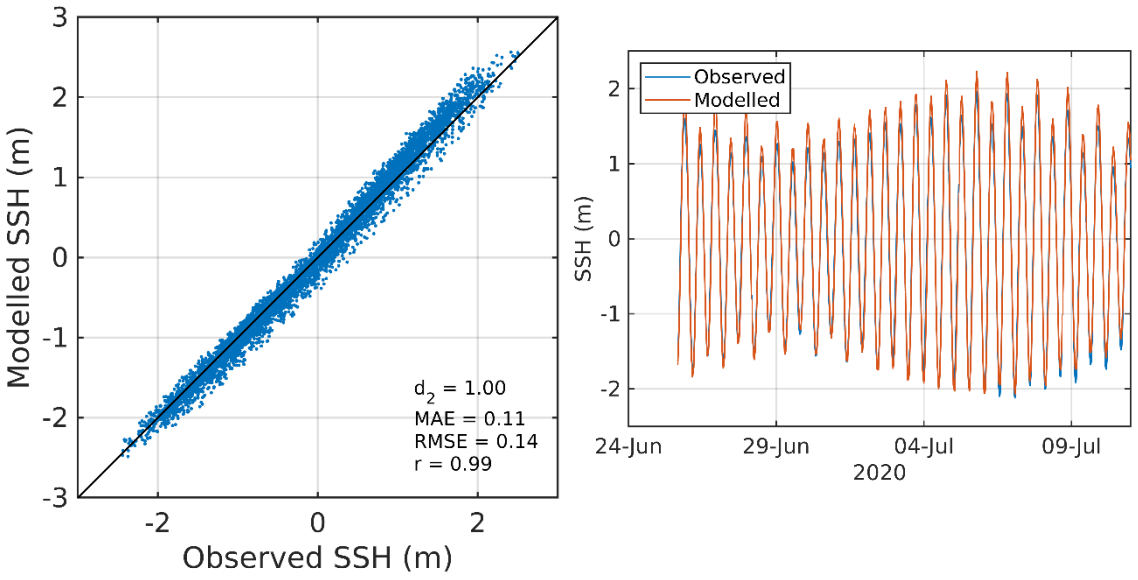

Figure 16. Comparison between observed and modelled sea surface height from ID347 using model parameter values from Table 1. Both the full record (left) and a subset of 15 days (right) are shown. In the latter, the observed data are in blue, model results in red.

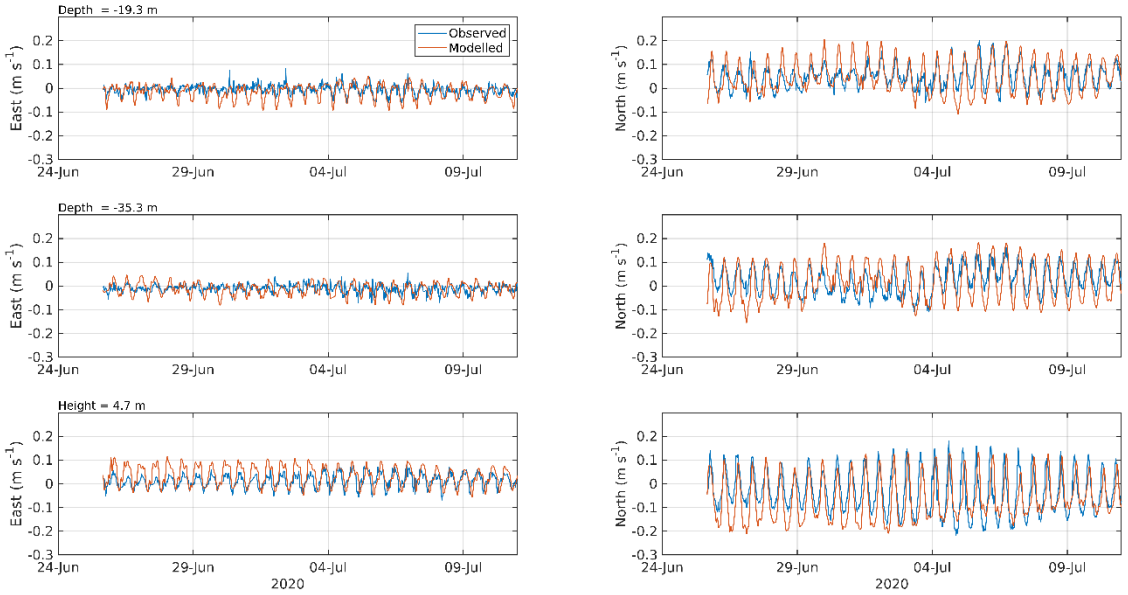

Figure 17. Comparison between observed and modelled East (left) and North (right) components of velocity at the ADCP location for 15 days in June – July 2020 (ID347) at three depths: 19.3 m (top), 35.3 m (middle) and 65.3 m (4.7 m above the seabed, bottom). Observed data are in blue, model results in red.

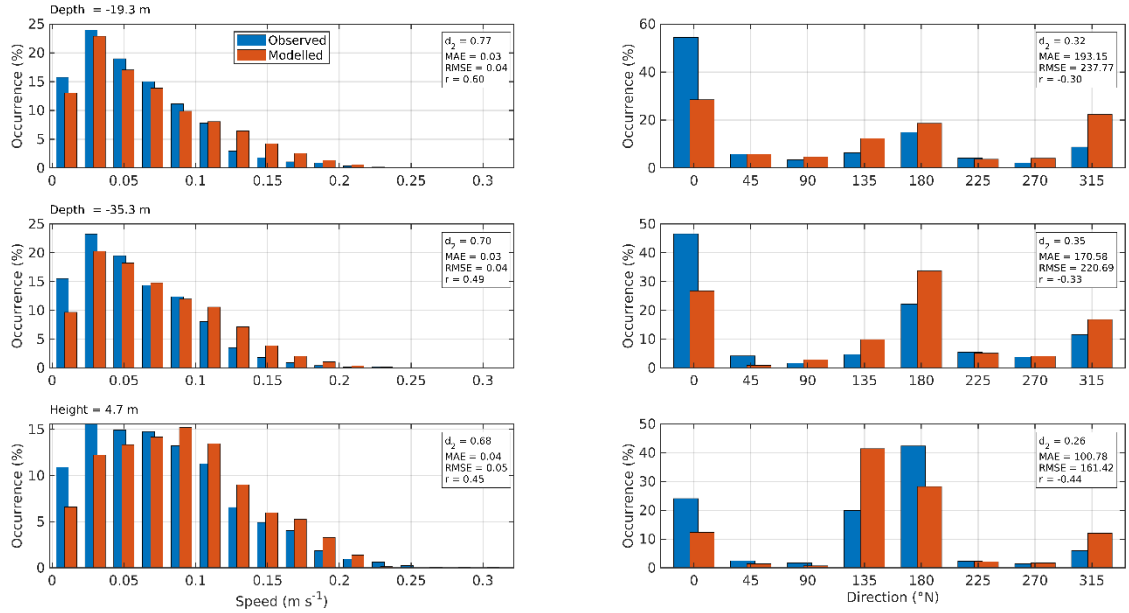

Figure 18. Histograms of observed and modelled speed (left) and direction (right) at the ADCP location for 15 days in June – July 2020 (ID347) at three depths: 19.3 m (top), 35.3 m (middle) and 65.3 m (4.7 m above the seabed, bottom). Observed data are in blue, model results in red.

Table 4. Model performance statistics for sea surface height (SSH) and East and North velocity at the ADCP location from 10 September – 08 November 2020 (ID347) at three depths (19.3 m, 35.3 m and 65.3 m).*

		Skill, d_2	MAE	RMSE
Sea Surface Height (SSH, m)		1.00	0.11	0.14
19.3 m	East Velocity (m s^{-1})	0.62	0.02	0.03
	North Velocity (m s^{-1})	0.86	0.04	0.05
35.3 m	East Velocity (m s^{-1})	0.58	0.02	0.03
	North Velocity (m s^{-1})	0.85	0.04	0.05
65.3 m*	East Velocity (m s^{-1})	0.71	0.03	0.03
	North Velocity (m s^{-1})	0.83	0.05	0.06

** estimated from mean water depth of 70.0 m*

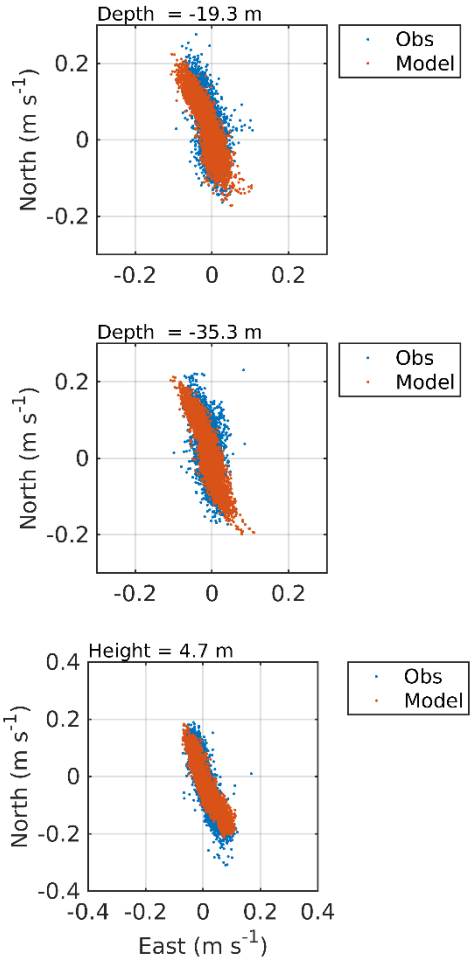

Figure 19. Scatter plot of observed and modelled velocity at the ADCP location for 15 days in June – July 2020 (ID347) at three depths: 19.3 m (top), 35.3 m (middle) and 65.3 m (4.7 m above the seabed, bottom). Observed data are in blue, model results in red.

4.4.2 ID348 (Seaforth)

The results of the validation exercise for ID348 are presented in Figure 20 – Figure 23 and Table 5. At the ADCP location, the sea surface height was accurately modelled, with model skill of 1.00. The mean absolute error (MAE) and root-mean-square error (RMSE) values of 0.11 m and 0.14 respectively are about 2.4% and 3.1% of the spring tide range respectively.

Model skill scores for the East and North components of uppermost (26.9 m) velocity were 0.80 and 0.83 respectively, with RMSE values of 0.03 m s^{-1} and 0.04 m s^{-1} for the two components of velocity respectively (Table 5). At the deeper depth of 46.9 m, the skill scores were similar, at 0.80 and 0.81 respectively. The RMSE values were the same as those at the shallower depth, at 0.03 m s^{-1} and 0.04 m s^{-1} respectively. At the deepest depth, 104.9 m, skill scores and RMSE values were similar to those at the shallower depths for both components of velocity.

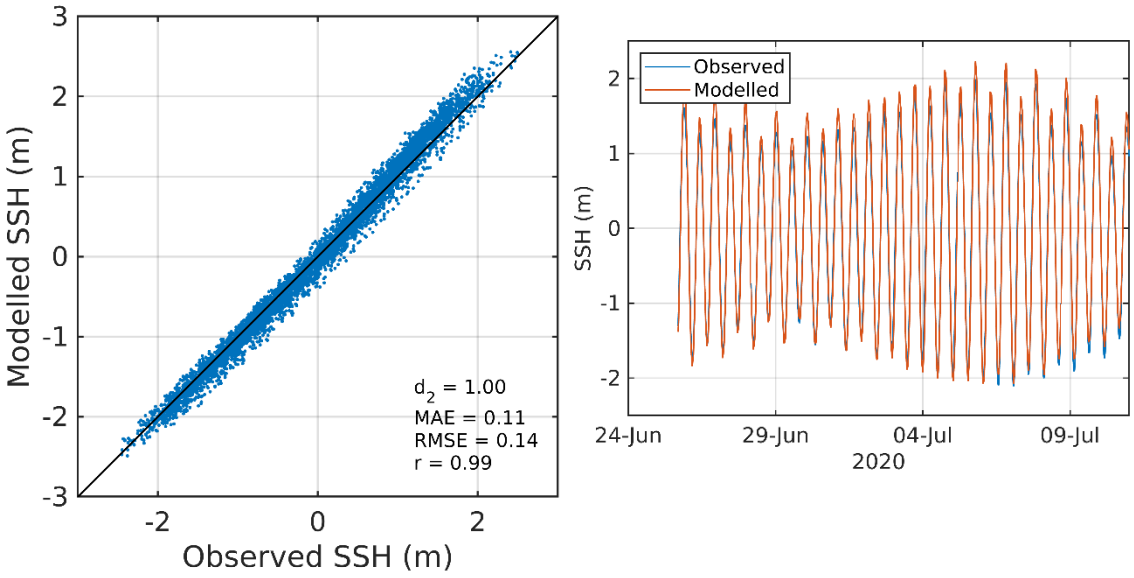

Figure 20. Comparison between observed and modelled sea surface height from ID348 using model parameter values from Table 1. Both the full record (left) and a subset of 15 days (right) are shown. In the latter, the observed data are in blue, model results in red.

Table 5. Model performance statistics for sea surface height (SSH) and East and North velocity at the ADCP location from 10 September – 08 November 2020 (ID348) at three depths (26.9 m, 46.9 m and 104.9 m).*

		Skill, d_2	MAE	RMSE
Sea Surface Height (SSH, m)		1.00	0.11	0.14
26.9 m	East Velocity (m s^{-1})	0.80	0.02	0.03
	North Velocity (m s^{-1})	0.83	0.03	0.04
46.9 m	East Velocity (m s^{-1})	0.80	0.02	0.03
	North Velocity (m s^{-1})	0.81	0.03	0.04
104.9 m*	East Velocity (m s^{-1})	0.79	0.04	0.05
	North Velocity (m s^{-1})	0.78	0.05	0.06

** estimated from mean water depth of 109.6 m*

The histograms and scatter plots (Figure 22 and Figure 23) demonstrate that the modelled current had broadly the same magnitude and direction characteristics as the observed data.

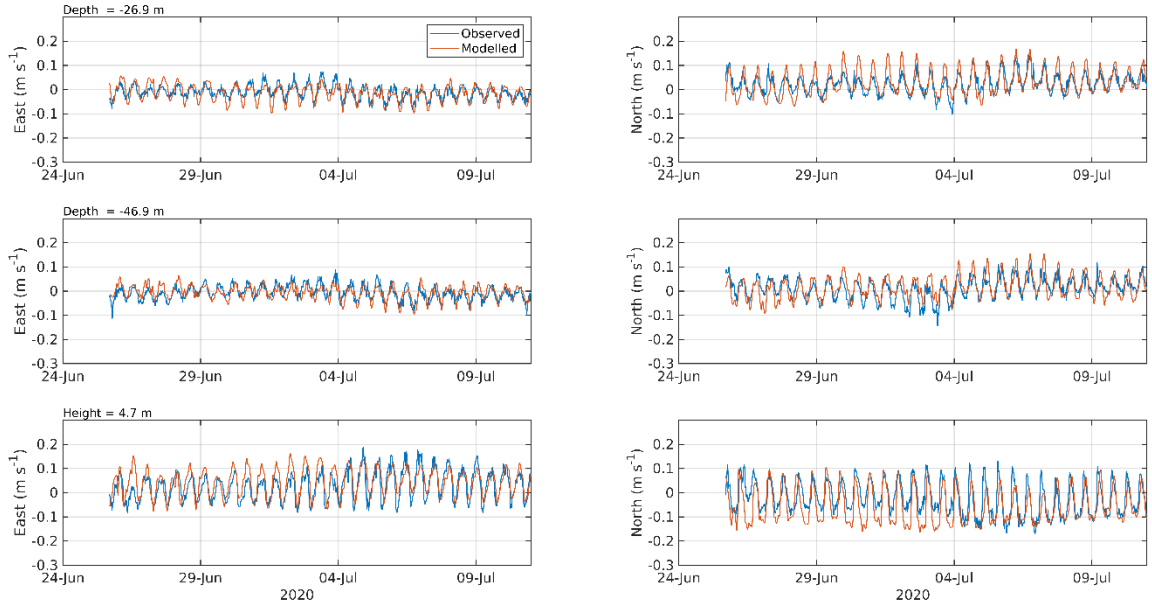

Figure 21. Comparison between observed and modelled East (left) and North (right) components of velocity at the ADCP location for 15 days in June – July 2020 (ID348) at three depths: 26.9 m (top), 46.9 m (middle) and 104.9 m (4.7 m above the seabed, bottom). Observed data are in blue, model results in red.

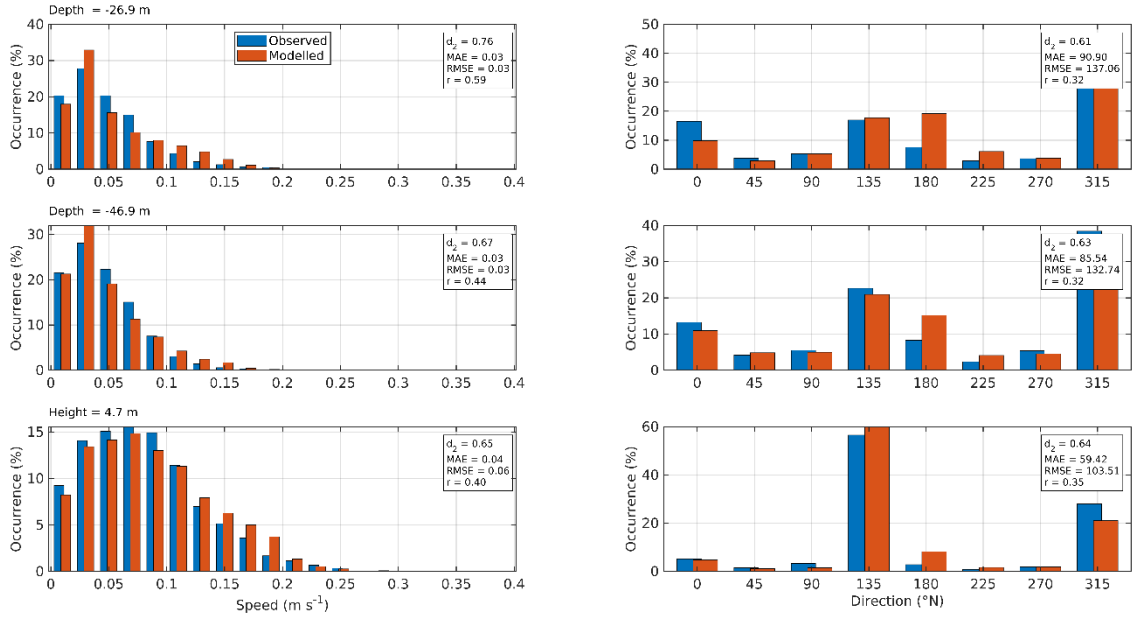

Figure 22. Histograms of observed and modelled speed (left) and direction (right) at the ADCP location for 15 days in June – July 2020 (ID348) at three depths: 26.9 m (top), 46.9 m (middle) and 104.9 m (4.7 m above the seabed, bottom). Observed data are in blue, model results in red.

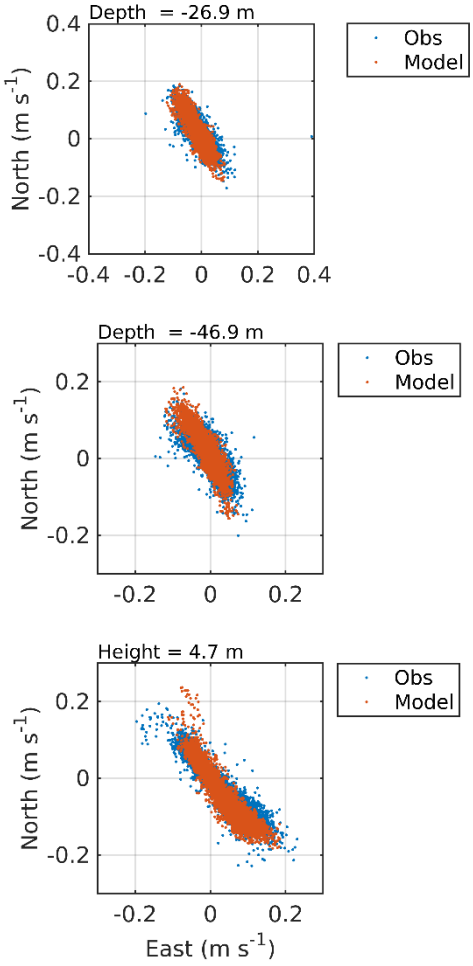

Figure 23. Scatter plot of observed and modelled velocity at the ADCP location for 15 days in June – July 2020 (ID348) at three depths: 26.9 m (top), 46.9 m (middle) and 104.9 m (4.7 m above the seabed, bottom). Observed data are in blue, model results in red.

5. Modelled Flow Fields

Modelled flood and ebb velocity vectors at spring tides are illustrated in Figure 24. Modelled velocity fields from layer 3 in the model (σ = 0.065, midway between sigma-levels 3 and 4) were used in Figure 24 and Figure 25. At the Trilleachan Mor site, where water depths were about 41.5 m, the depth of the plotted velocity vectors was therefore about 2.7 m; clearly the depth of the plotted vectors varies spatially as the water depths in the loch vary.

Modelled near-surface currents at spring tides reached speeds of up to 40 cm s^{-1} (Figure 24), being stronger on the ebb tide than on the flood, as expected in a stratified sea loch. In the flood tide snapshot shown, near-surface currents are being steered up the eastern arm of the loch; on the ebb, currents are flowing seawards down both arms to the north of the site. During ebb tides, modelled currents speeds were somewhat weaker than during spring tides.

The mean (residual) near-surface currents are seaward within Loch Seaforth (Figure 25), again as expected in a stratified sea loch. The model indicates a predominantly seaward (southward)

near-surface flow, with mean speeds up to around 10 cm s^{-1}. The observed near-surface residual current speed at Trilleachan Mor (deployment ID440) was 3.8 cm s^{-1} (Mowi, 2024). These residual flows indicate that patches of medicine following treatment at Trilleachan Mor will be transported southwards into the open waters of the Minch, where dispersion and dilution is likely to be rapid.

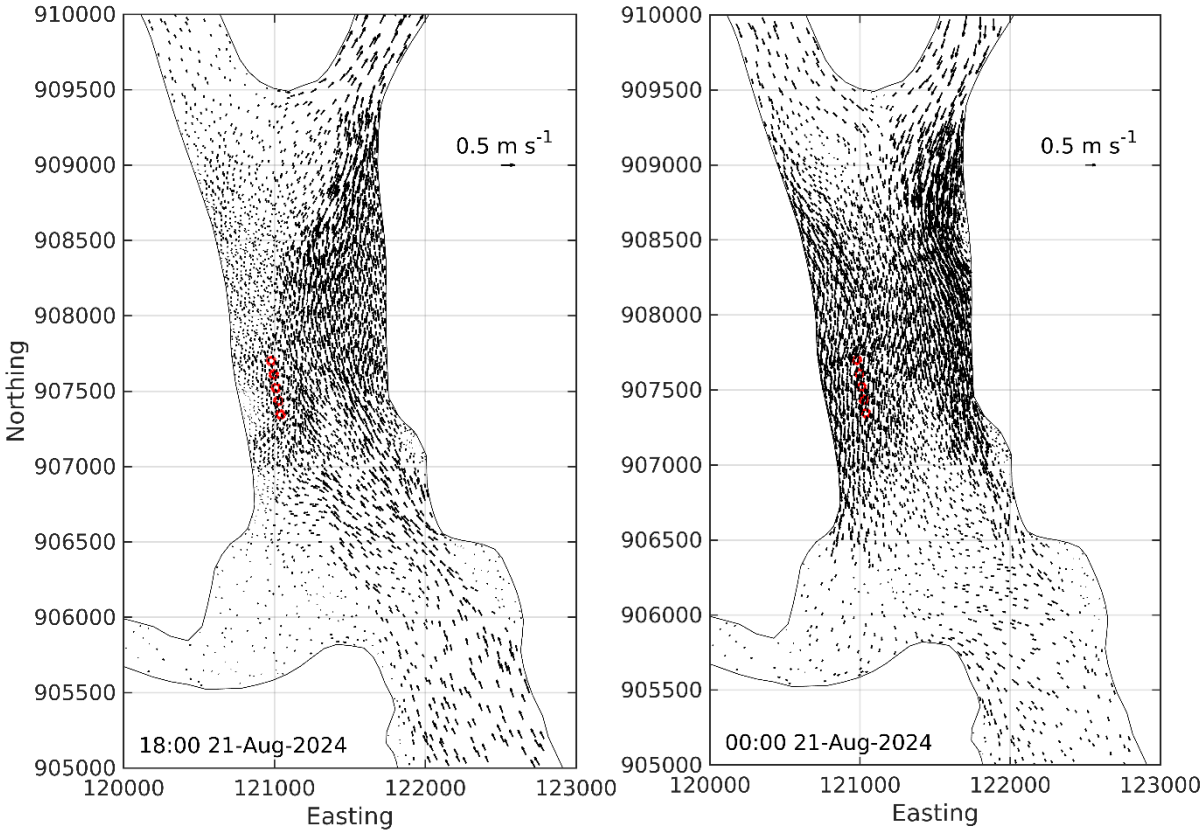

Figure 24. Modelled flood (left) and ebb (right) near-surface current vectors at Trilleachan Mor during spring tides on 21st August 2024 at 18:00Z and 00:00Z respectively.

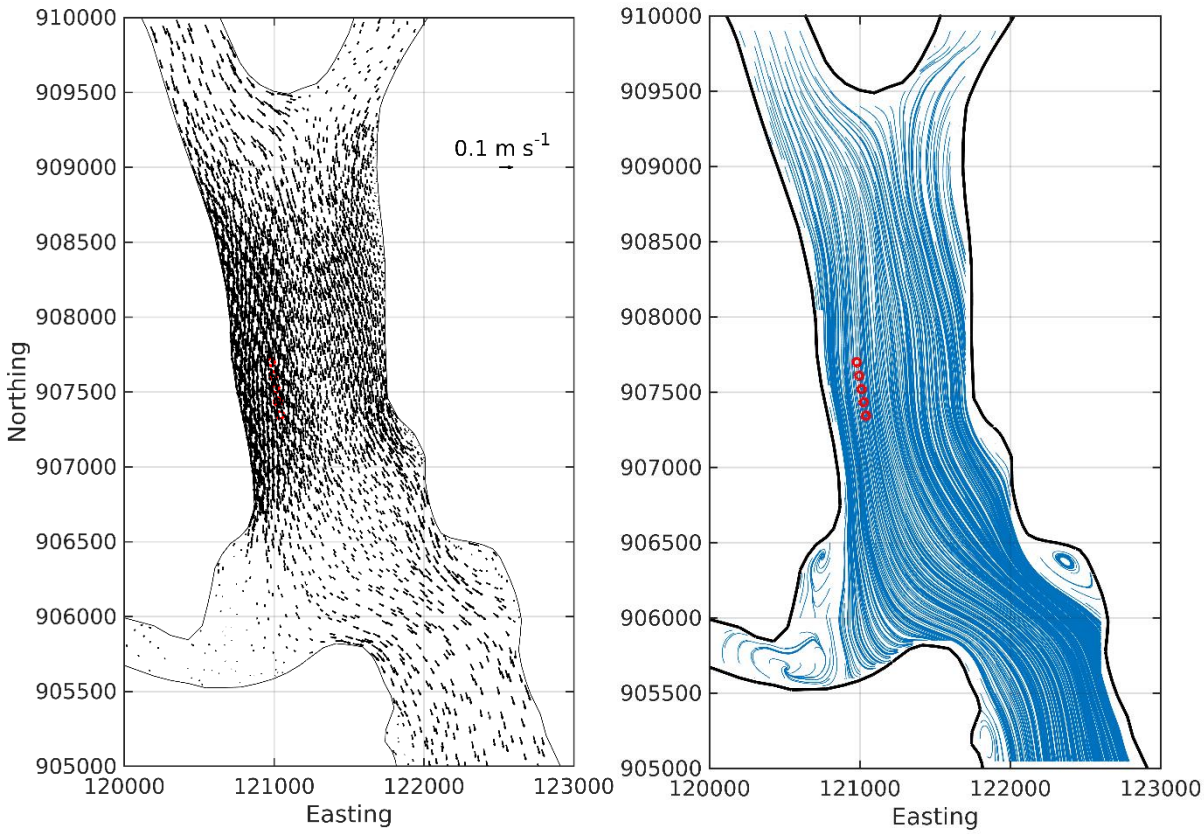

Figure 25. Modelled mean (residual) near-surface current vectors (left) and streamlines (right) at Trilleachan Mor, averaged over the full simulation from 18th June – 21st September 2024.

6. Conclusions

This report demonstrates that the hydrodynamic model of Loch Seaforth adequately reproduces the measured currents in Loch Seaforth at four locations (and three time periods) along the length of the loch. The magnitude and direction of the modelled currents at all depths is broadly correct. In addition, the near-surface residual flows at Trilleachan Mor, which will determine the net transport of discharges, are accurately simulated. We conclude that the model is suitable for simulating the transport and dispersion of bath medicines from Trilleachan Mor.

7. References

Burchard, H., 2002. Applied turbulence modeling in marine waters. Springer:Berlin-Heidelberg-New York-Barcelona-Hong Kong-London-Milan Paris-Tokyo, 215pp.

Chen, C., H. Liu, and R.C. Beardsley, 2003. An unstructured, finite-volume, three-dimensional, primitive equation ocean model: Application to coastal ocean and estuaries. J. Atmos. Ocean. Tech., 20, 159 – 186.

Edwards, A. and Sharples, F., 1986. Scottish Sea Lochs: A Catalogue. Scottish Marine Biological Association, Dunstaffnage Marine Laboratory, Oban, U.K., 400pp.

ECMWF, 2021. ERA5 Dataset, European Centre for Medium-Range Weather Forecasts. Available at https://www.ecmwf.int/en/forecasts/datasets/reanalysis-datasets/era5

Gillibrand, P.A., Walters, R.A., and McIlvenny, J., 2016. Numerical simulations of the effects of a tidal turbine array on near-bed velocity and local bed shear stress. *Energies*, vol 9, no. 10, pp. 852. DOI: 10.3390/en9100852

Large. W.G. and Pond, S., 1981. Open ocean momentum flux measurements in moderate to strong winds. J. Phys. Oceanogr., 11, 324—336.

Marine Scotland, 2016. Scottish Shelf Model. Part 4: East Coast of Lewis and Harris Sub-Domain. Available at https://www.gov.scot/publications/scottish-shelf-model-part-4-east-coast-lewis-harris-sub/pages/4/

Mowi, 2024.Trilleachan Mor, Loch Seaforth. Hydrographic Data Report: Deployment ID440. Mowi Scotland Ltd. report, December 2024, 15 pp.

Umlauf, L.; Burchard, H. 2003. A generic length-scale equation for geophysical turbulence models, J. Mar. Res., 61, 235-265.

Walters, R.A.; Casulli, V., 1998. A robust, finite element model for hydrostatic surface water flows. Comm. Num. Methods Eng., 14, 931–940.

Warner, J.C.; Sherwood, C.R.; Arango, H.G.; Signell, R.P.; 2005. Performance of four turbulence closure models implemented using a generic length scale method. Ocean Modelling, 8, 81 – 113.

Willmott, C. J.; Ackleson, S. G.; Davis, R. E.; Feddema, J. J.; Klink, K. M.; Legates, D. R. O'Donnell, J.; Rowe, C. M. 1985. Statistics for evaluation and comparison of models, J. Geophys. Res., 90, 8995– 9005.